Efficient and temperature-independent terahertz emission from CoFeB/NiCu heterostructures

Hao Cheng,[1] Yangkai Wang,[1] Hongchuan He,[1] Qiuping Huang,[2,*] and Yalin Lu[2,†]

[1]*Department of Materials Science and Engineering, University of Science and Technology of China, Hefei, Anhui 230026, People's Republic of China*

[2]*Hefei National Laboratory for Physical Sciences at the Microscale and Anhui Laboratory of Advanced Photon Science and Technology, University of Science and Technology of China, Hefei 230026, People's Republic of China*

(Received 16 December 2021; revised 19 March 2022; accepted 12 April 2022; published 21 April 2022)

Spintronic terahertz (THz) emission has been investigated in ferromagnetic (FM) metal/nonmagnetic (NM) metal, FM/semiconductor, and FM/topological insulator systems. However, THz emission in the heterojunction of FM and 3*d* transition light metal is rarely reported. Large spin Hall angles have been observed in a light metal alloy of the 3*d* transition metal NiCu, allowing for the emission of high-performance THz waves without the use of heavy metal. Here, we present a comprehensive study of THz emission from a CoFeB/NiCu heterostructure, with peak intensity of emitted THz pulses up to half that of CoFeB/Pt. The THz radiation from CoFeB/NiCu is shown to be generated by the spin-to-charge conversion in NiCu via the inverse spin Hall effect. The evolution of the THz signal of CoFeB/$Ni_{70}Cu_{30}$ across $Ni_{70}Cu_{30}$ Curie temperature is also explored, and it is discovered that the THz emission signal in this sample is temperature independent and unaffected by the magnetic state of $Ni_{70}Cu_{30}$. Our findings highlight the great potential of light metal alloys containing 3*d* transition elements as spintronic THz emitters. Moreover, it has been demonstrated that THz emission spectroscopy is a helpful tool for investigating inverse spin Hall effect or anomalous Hall effect in ferromagnets.

DOI: 10.1103/PhysRevB.105.155141

I. INTRODUCTION

Terahertz wave shows frequencies in the resonance windows of many materials, which makes great potential applications in material analysis, imaging, communication, and spectroscopy, etc. [1–5]. The development of high-performance THz sources is still a hot topic in THz technology. Traditional THz waves are commonly generated by transient electrical currents in photoconductive antennas [6–9], optical rectification from electro-optical crystals [10–12], and plasma oscillations [13–15]. Spintronic THz emission based on spin-to-charge conversion has recently received a lot of attention due to its advantages in terms of intensity, bandwidth, and low manufacturing costs [16–18]. This spin-to-charge conversion is mostly based on the heterojunction structure of ferromagnetic (FM) and nonmagnetic (NM) thin films, via inverse spin Hall effect (ISHE) [19,20] and inverse Rashba-Edelstein effect (IREE) [21–23], radiating THz wave. The FM/NM system has been the subject of previous research. The NM layer is mainly composed of heavy metals with large spin Hall angles (SHAs), such as Pt, W, Ta, and Ir [16–18,24,25]. Aside from heavy NM metallic materials, other materials with an inverse spin Hall effect have been studied in spintronic THz radiation, including semiconductors [26,27], topological insulators [28], and even light metals [29]. However, the intensity of THz signals from light metals is much lower than that of heavy metals due to the low spin-orbit coupling (SOC) of light metals. For example, the THz signal emitted by a Co/Al heterostructure is roughly one-third that of a Co/Pt heterostructure [29]. It is still worth looking for a light metal with a higher spin-to-charge conversion in the spintronic THz emitter.

In general, SOC in light metals is typically low. However, a light metal alloy of 3*d* transition metal NiCu can achieve a high SHA of 4.1%, comparable to Pt [19,30–33]. Therefore, high-performance THz radiation can be generated in NiCu metal using ISHE. Furthermore, the Curie temperature of NiCu metal is sensitive to compositional stoichiometry [34]. And the NiCu is in the paramagnetic state above the Curie temperature (T_c), while below T_c it is in the ferromagnetic phase [30–32]. Therefore, NiCu is an excellent material for studying THz emission in the FM/FM system, which has received little attention. In addition, in ferromagnetic metals, the link between the spin Hall effect (SHE) and the magnetic order has been reported with different results [31,32]. THz emission spectroscopy (TES) may be useful for analyzing the effect of the ferromagnetic-paramagnetic transition on the SHE/ISHE because TES is an appealing technique for studying ultrafast spin dynamics with subpicosecond time resolution [35–37].

In this work, we investigate the THz emission from a light metal alloy of 3*d* transition metal NiCu based on the CoFeB/NiCu structure. The $Co_{40}Fe_{40}B$ is used to generate spin current under femtosecond laser irradiation, while the NiCu layer converts spin to charge, radiating the THz wave. The maximal THz amplitude from CoFeB/$Ni_{70}Cu_{30}$ is found to be nearly half that of CoFeB/Pt. It is demonstrated that the THz radiation from CoFeB/NiCu is generated by the

*qphuang@ustc.edu.cn
†yllu@ustc.edu.cn

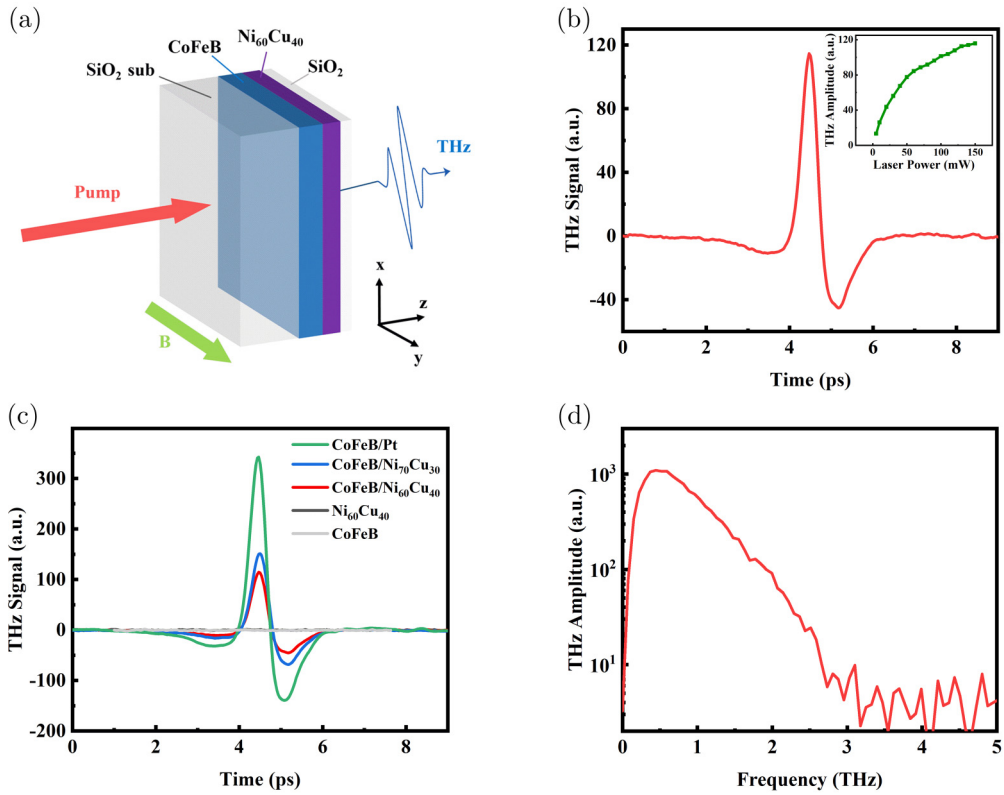

FIG. 1. (a) Schematic illustration of THz emission from CoFeB/NiCu heterostructure. The sample is excited by a femtosecond laser beam with 800 nm wavelength and 35 fs pulse duration along the z axis from the SiO_2 substrate side. An external magnetic field with 70 mT is applied to orient the magnetic of CoFeB along the y axis. (b) The typical THz pulse emitted from the CoFeB/NiCu heterostructure detected by the electro-optical sampling of the 500-μm-thick ZnTe(110) crystal. The inset shows the THz emission dependent on the incident laser power from the $CoFeB/Ni_{60}Cu_{40}$ heterostructure. (c) THz wave forms emitted from CoFeB/Pt, $CoFeB/Ni_{60}Cu_{40}$, $CoFeB/Ni_{70}Cu_{30}$, NiCu film, and CoFeB film, respectively. (d) Fourier-transformed spectrum of (b).

spin-to-charge conversion via the inverse spin Hall effect in NiCu. The evolution of the THz signal of $CoFeB/Ni_{70}Cu_{30}$ across Curie temperature of $Ni_{70}Cu_{30}$ is also investigated, and it is realized that the THz signal in this sample is insensitive to the magnetic state of $Ni_{70}Cu_{30}$. We also replaced the CoFeB layer with Ni having a large SHA and demonstrated that the CoFeB/NiCu structure is insensitive to the temperature because the SHA of CoFeB is small. This study shows that light metal alloys of 3d transition elements with large spin Hall angles have potential as spintronic THz emitters in both their paramagnetic and ferromagnetic phases. THz emission spectroscopy, on the other hand, can be used to study the ISHE in ferromagnets.

II. EXPERIMENT

Figure 1(a) shows the schematic of the device structure. The CoFeB/NiCu heterostructure was grown on a 500-μm-thick SiO_2 substrate by magnetron sputtering. The pressure of the sputtering chamber was below 2×10^{-6} mTorr. For the ferromagnetic layer, we choose the $Co_{40}Fe_{40}B$ because it is a good spin injector. Two kinds of NiCu thin films were sputtered on top of CoFeB from $Ni_{60}Cu_{40}$ and $Ni_{70}Cu_{30}$ targets, respectively. The sample was further protected by a 2–3 nm SiO_2 layer. The thicknesses of the CoFeB and NiCu layers range from 1 to 14 nm. A femtosecond laser beam with 800 nm wavelength and 35 fs pulse duration was incident on the device along the z axis. The excited beam spot size is about 3 mm in diameter and 100 mW in power. An external magnetic field (B) of 70 mT was applied to orient the magnetic of CoFeB along the y axis. Terahertz radiation emitted from the sample with the electric field along the x axis was detected by the 500-μm-thick ZnTe (110) crystal. The THz emission experiment was performed at room temperature in a dry air atmosphere. For temperature dependence experiment, the $CoFeB/Ni_{70}Cu_{30}$ sample was put in a cryostat with optical windows and cooled by liquid nitrogen. More experimental details can be seen in Sec. I of the Supplemental Material [38].

III. RESULTS

Figure 1(b) shows a typical THz pulse emitted from the CoFeB (4 nm)/$Ni_{60}Cu_{40}$ (6 nm) heterostructure, with the peak at 4.5 ps. The Fourier-transformed spectrum of the time-domain signal is plotted in Fig. 1(d), covering the frequency region of 3 THz, which is limited by the electro-optical detection of a 0.5-mm-thick ZnTe crystal. The inset of Fig. 1(b) depicts the THz emission from a $CoFeB/Ni_{60}Cu_{40}$ heterostructure as a function of incident laser power. The results show a linear power dependence below 50 mW and saturation behavior above 50 mW. We also measured the THz emission from the CoFeB (4 nm)/Pt (4 nm) structure, as well

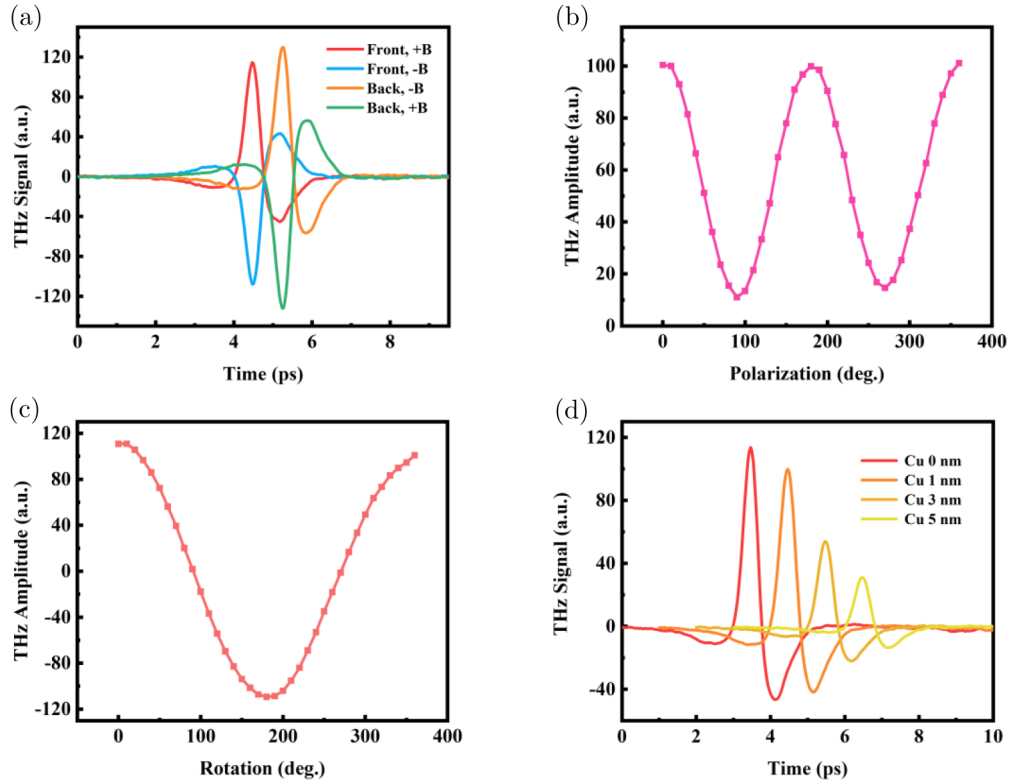

FIG. 2. (a) THz emissions emitted from the CoFeB (4 nm)/$Ni_{60}Cu_{40}$ (6 nm) heterostructure measured with excitation on the side of substrate (front) and films (back) and reversed magnetic field. (b) THz peak amplitude emitted from the CoFeB(4 nm)/$Ni_{60}Cu_{40}$ (6 nm) as a function of polarizer angle θ. (c) THz peak amplitude emitted from the CoFeB (4 nm)/$Ni_{60}Cu_{40}$ (6 nm) as a function of magnetic field rotation angle Φ with respect to the positive y axis. (d) THz emissions from the CoFeB (4 nm)/Cu(d_{Cu})/$Ni_{60}Cu_{40}$ (6 nm) samples, where $d_{Cu} = 0$, 1, 3, and 5 nm. The data are shifted horizontally for clarity.

as the single NiCu and CoFeB films protected by the SiO_2 film, for comparison. As shown in Fig. 1(c), THz signals from all heterostructure samples revealed similar features, with the peak at ≈4.5 ps. The amplitude of CoFeB/$Ni_{60}Cu_{40}$ is about one-third of that of CoFeB/Pt. We find that the THz amplitude from CoFeB/$Ni_{70}Cu_{30}$ is nearly half that of CoFeB/Pt, demonstrating effective THz emission from 3*d* transition metals. Furthermore, no obvious THz signal is observed in the isolated NiCu and CoFeB films. It implies that THz waves are generated by the bilayer structure of CoFeB/NiCu.

We use CoFeB/$Ni_{60}Cu_{40}$ stacks as a sample to further investigate the properties of the emitted THz wave. At room temperature, the $Ni_{60}Cu_{40}$ (Curie temperature $T_c \approx$ 210 K [32]) film is in the paramagnetic phase, and thus the CoFeB/NiCu bilayers belong to the FM/NM heterostructure system. In this case, THz emission is generated by spin-to-charge conversion via either the ISHE in the bulk or the IREE on the surface. The following is an explanation of the procedure. To begin with, a femtosecond pulse is injected into the FM layer, causing spin-polarized currents to be excited due to differences in mobility between the majority and minority spins. The spin-polarized currents then reach the NiCu film and are converted to ultrafast charge currents by the ISHE or IREE, resulting in THz emission. In ISHE, $\boldsymbol{j_c} \propto \theta_{SHE}\, \boldsymbol{j_s} \times \boldsymbol{M}$, where $\boldsymbol{j_c}$ is the charge current, θ_{SHE} is the spin Hall angle of NM, $\boldsymbol{j_s}$ is spin current, and $\boldsymbol{M}$ is the magnetization of the FM layer [16]. In IREE, $\boldsymbol{j_c} \propto \lambda_{IREE}\, \boldsymbol{j_s} \times \hat{\boldsymbol{z}}$, where λ_{IREE} is the IREE coefficient and $\hat{\boldsymbol{z}}$ is the direction of the potential gradient perpendicular to the interface [39]. The polarization of the THz wave emitted by ISHE and IREE is relative to the magnetization of the sample.

We altered the in-plane magnetization of the sample to modify the spin polarization injected into the NiCu layer. As illustrated in Fig. 2(a), when reversing the magnetic field, the phase of the THz wave shifts 180°, indicating the phase of the THz wave shows a high dependence on the magnetic field. It is noted that amplitude and time delay of THz emissions are different when exciting the samples from the side of the substrate and the films, which originates from the different refractive indices of the SiO_2 substrate in the 800 nm and THz frequency range. The THz wave phase also shows dependence with the order of CoFeB and NiCu stacks as the pump beam incidents on the opposite side of the sample due to changing the direction of spin current pumped to NiCu film. The THz peak amplitude, as plotted in Fig. 2(c), is dependent on the angle Φ of magnetic field direction with respect to the positive y axis and exhibits simple cosine curve behavior. The THz peak amplitude transmitted through an analyzing polarizer with a rotating angle θ is shown in Fig. 2(b). The intensity of the THz peak amplitude follows the $\cos^2\theta$ behavior, with the maximum at $\theta = 90°$ and 270°, indicating that the emitted THz field is linear and p polarized.

The results presented above are consistent with the characteristics of spintronic THz emission. ISHE and IREE can perform the spin-to-charge conversion. And IREE occurs at the interfaces with broken inversion symmetry and ISHE

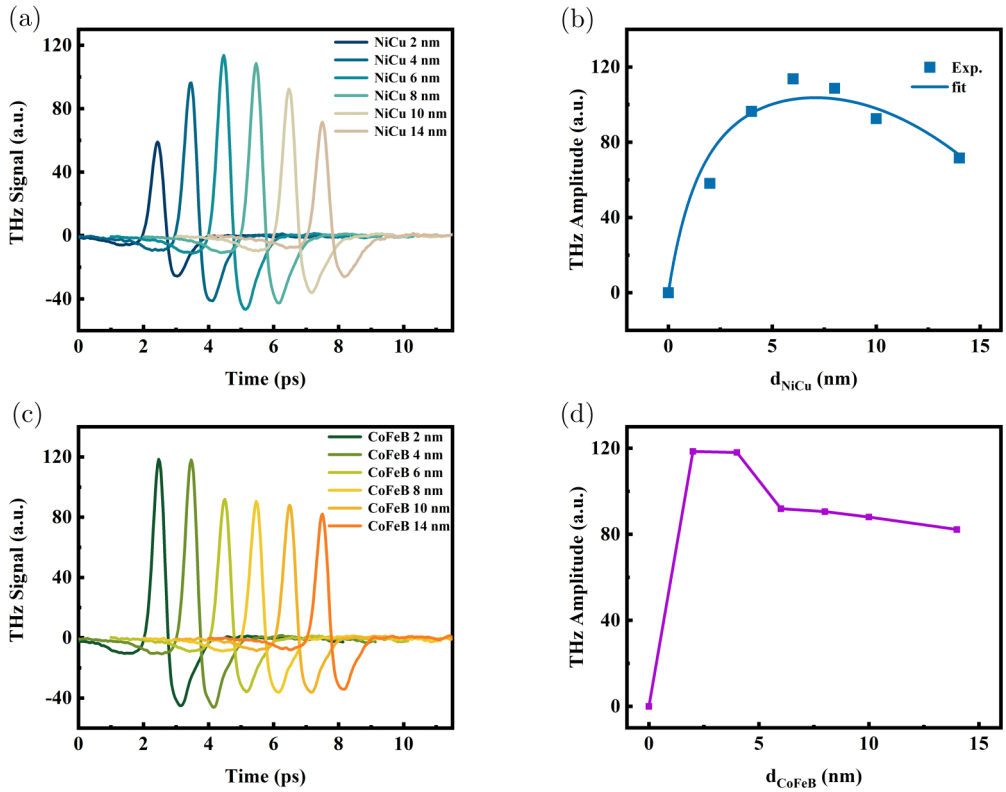

FIG. 3. (a) THz pulses emitted from CoFeB (4 nm)/$Ni_{60}Cu_4$(d_{NiCu}), where $d_{NiCu} = 2$, 4, 6, 8, 10, and 14 nm. The data are shifted horizontally for clarity. (b) The THz peak amplitudes dependent on the thickness of NiCu films for CoFeB/$Ni_{60}Cu_{40}$. The line denotes the fitted result. (c) THz pulses emitted from CoFeB(d_{CoFeB})/$Ni_{60}Cu_{40}$ (6 nm), where $d_{CoFeB} = 2$, 4, 6, 8, 10, and 14 nm. The data are shifted horizontally for clarity. (d) The dependence between CoFeB thickness and THz peak amplitude for CoFeB/$Ni_{60}Cu_{40}$.

happens in the bulk of the metallic system with SOC. To explore the mechanism of spin-to-charge conversion in NiCu, we inserted a layer of Cu film between the CoFeB and NiCu layers. Due to the spin-diffusion length of a hundred nanometers, spin current can efficiently transmit through the thin Cu film. In this scenario, the effect of ISHE will not be affected much. Nevertheless, the Cu separator disrupts the CoFeB/NiCu interface and significantly impacts the interface-related effect of IREE. The THz emissions of CoFeB (4 nm)/Cu (d_{Cu})/NiCu (6 nm) are shown in Fig. 2(d). When the thickness of the Cu layer is increased, the THz signal is attenuated. The decrease in THz signal is attributed to the loss of spin current in the Cu layer. It is clear that the intensities of THz amplitudes are still high in the presence of Cu films. Because the Cu layer is thick enough to destroy the initial interface, the IREE effect on spin-to-charge conversion is eliminated. In other words, the ISHE primarily contributes to the THz wave emitted by CoFeB/NiCu.

Next, we analyze the relationship between THz emission and the thicknesses of the NiCu layer and the CoFeB layer. We fixed the CoFeB thickness at 4 nm and deposited the NiCu films with a thickness that varied from 2 to 14 nm. THz emissions from CoFeB (4 nm)/NiCu (d_{NiCu}) are shown in Fig. 3(a), and the THz peak amplitude as a function of NiCu thickness is plotted in Fig. 3(b). The THz peak amplitude increases with increasing NiCu thickness and then decreases with a maximum amplitude at $d_{NiCu} = 6$ nm. This result is consistent with the common FM/NM system. Such behavior can be explained by the spin diffusion in the NiCu layer. As the NiCu thickness increases, spin currents can diffuse further and more charge currents can be generated in the bulk, increasing the THz emission. However, as the NiCu thickness increases, the sample impedance decreases, reducing the THz emission significantly. In order to achieve the spin-diffusion length of $Ni_{60}Cu_{40}$, we used the model in Ref. [29] to fit the THz emissions as a function of the thickness of $Ni_{60}Cu_{40}$. And the calculated spin-diffusion length is $\lambda_{NiCu} = 0.2 \pm 0.2$ nm. This spin-diffusion length, however, is an order of magnitude shorter than that reported in the gigahertz regime with ferromagnetic resonance measurements [30,32].

Furthermore, we fixed the NiCu thickness at 6 nm and changed the CoFeB thickness. As shown in Figs. 3(c) and 3(d), the THz peak amplitude reaches a maximum at $d_{CoFeB} =$ 2 nm and then decreases with increasing CoFeB thickness. This is due to laser-induced spin diffusion and THz optical absorption in the CoFeB layer.

Furthermore, we investigate the temperature dependence of THz emission from the CoFeB (4 nm)/$Ni_{70}Cu_{30}$ (4 nm) heterostructure. We used a cryostat to cool the sample from room temperature to 130 K. Figure 4(a) depicts the THz radiation emitted by a CoFeB (4 nm)/$Ni_{70}Cu_{30}$ (4 nm) heterostructure at various temperatures. Figure 4(b) shows the THz peak amplitude as a function of temperature; there is no discernible change in THz intensity with temperature. Figure 4(c) shows the M-T curve of $Ni_{70}Cu_{30}$ films, displaying the Curie temperature (T_c of $\sim 250 \pm 10$ K). Therefore, the

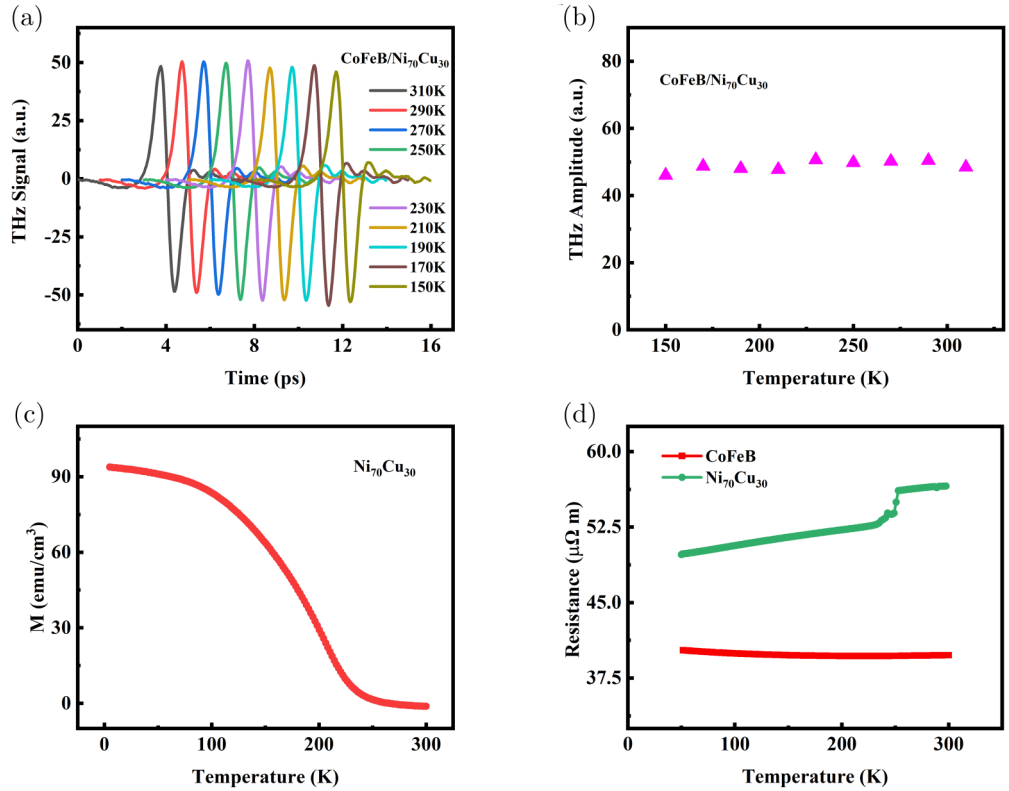

FIG. 4. (a) THz pulses emitted from the CoFeB (4 nm)/$Ni_{70}Cu_{30}$ (4 nm) sample measured under different temperatures. The data are shifted horizontally for clarity. (b) Temperature dependence of THz peak amplitude of the CoFeB (4 nm)/$Ni_{70}Cu_{30}$ (4 nm) sample. (c) Saturation magnetic moment vs temperature (M-T curves) for $Ni_{70}Cu_{30}$ (10 nm). (d) The resistance as a function of temperature of 4-nm-thick CoFeB and $Ni_{70}Cu_{30}$ layers, respectively.

$Ni_{70}Cu_{30}$ film undergoes a phase transition from paramagnetic to ferromagnetic in the temperature range of 290–130 K. At room temperature, the $Ni_{70}Cu_{30}$ film is in the paramagnetic state, and below the Curie temperature, the $Ni_{70}Cu_{30}$ film is in the ferromagnetic phase. As a consequence, at low temperatures, the THz emission from the FM/FM heterostructure has an intensity equal to that of the FM/NM state.

In the case of CoFeB film, Gilbert damping, magnetization, and resistivity are nearly temperature independent in the studied temperature range [40], and its self-induced SHE is small [41], thus the laser producing spin current in the CoFeB layer is unaltered. The resistivity of the $Ni_{70}Cu_{30}$ layer decreases with decreasing temperature, but the relative change is fairly small, as seen in Fig. 4(d). We believe that this minor variation in resistivity has little influence on terahertz emission. Therefore, the temperature-insensitive THz emission, the spin-to-charge conversion via ISHE in NiCu, is likewise temperature independent. We conclude that the ISHE is unaffected by the magnetic order in NiCu, which is consistent with recent studies done utilizing ferromagnetic resonance (FMR) [32]. This phenomenon may be explained by the similarity of the band structure of NiCu in the paramagnetic and ferromagnetic phases.

The spin Hall angle influences the THz signal emitted by spintronic THz emission. In Ref. [32], the spin Hall angle of NiCu is $\theta_{SHE} = 4.1\%$, which is comparable to Pt [19,32,33]. As a result, the intensity of the THz signal from NiCu is stronger than that of common light metals. Keller *et al.* evaluated the spin Hall effect in Ni_xCu_{1-x} for $x \in \{0.3, 0.75\}$ and found that the spin-orbit torque conductivity is greatest for alloys approaching $x = 0.7$. This finding could explain why the THz signal from CoFeB/$Ni_{70}Cu_{30}$ is stronger than CoFeB/$Ni_{60}Cu_{40}$ in our experiment.

In contrast to prior work conducted using FMR [32], the THz signal remains unaltered even when CoFeB is in direct contact with NiCu and below T_c. In the previous FMR measurement, it is found that the exchange coupling between the CoFeB and NiCu makes the magnetization vectors precess together at resonance, thus the resonance field and linewidth are modified. For the THz spintronic emission based on the femtosecond laser pump, the transport of spin-polarized electrons from the CoFeB into the NiCu form the spin current, and the THz emission is achieved by the ISHE of NiCu. In this case, the THz emission signal is related to the in-plane magnetization of the CoFeB layer. We measured the in-plane magnetic hysteresis loops (M-H curve) of CoFeB/$Ni_{70}Cu_{30}$ at 300 and 150 K, and the in-plane magnetic moment of CoFeB/$Ni_{70}Cu_{30}$ under a magnetic field of 70 mT, with results shown in Sec. IV of thebSupplemental Material [38]. It is found that the effect of exchange interaction between CoFeB and NiCu on the in-plane magnetization of CoFeB/$Ni_{70}Cu_{30}$ is weak and negligible in our example. And the in-plane magnetization of CoFeB in the CoFeB/$Ni_{70}Cu_{30}$ is temperature independent, leading to temperature-independent THz emission.

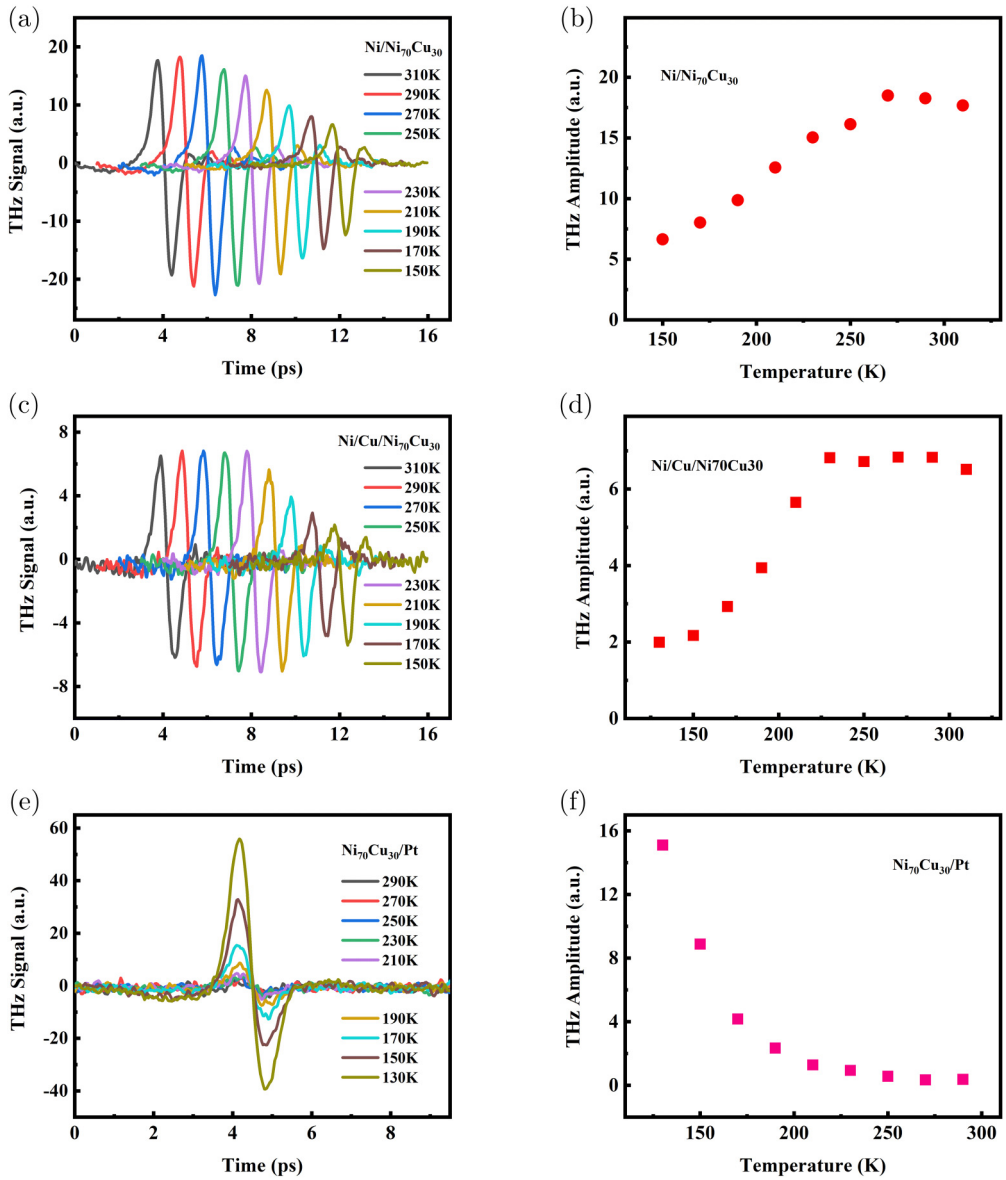

FIG. 5. THz pulses and THz peak amplitude measured under different temperature emitted from the Ni (4 nm)/$Ni_{70}Cu_{30}$ (4 nm) (a) and (b), from the Ni (4 nm)/Cu (5 nm)/$Ni_{70}Cu_{30}$ (c) and (d), and from the $Ni_{70}Cu_{30}$ (4 nm)/Pt (4 nm) (e) and (f). The data in (a) and (c) are shifted horizontally for clarity.

Additionally, to explore more effects of the ferromagnetic phase transition of NiCu on the THz emission, we replaced the CoFeB layer with Ni with a large SHA and investigated the temperature-dependent THz emission from the Ni (4 nm)/$Ni_{70}Cu_{30}$ (4 nm), Ni (4 nm)/Cu (5 nm)/$Ni_{70}Cu_{30}$ (4 nm), and $Ni_{70}Cu_{30}$ (4 nm)/Pt (4 nm) structures, respectively. From Fig. 5(f), it is obvious that the THz emission of the $Ni_{70}Cu_{30}$ (4 nm)/Pt (4 nm) structure increases with the decreasing temperature. And the turning temperature is around 250 K, which is the Curie temperature of $Ni_{70}Cu_{30}$. The magnetism of $Ni_{70}Cu_{30}$ is stronger at low temperatures, and so is the THz emission. It demonstrates that a $Ni_{70}Cu_{30}$ layer can generate spin currents at low temperatures, which may then be converted into charge currents and used to generate THz radiation when the adjacent layer has a high SOC.

The THz wave signal emitted by the Ni (4 nm)/$Ni_{70}Cu_{30}$ (4 nm) heterostructure at different temperatures is shown in Fig. 5(a). Figure 5(b) depicts the temperature-dependent peak THz signal. When the temperature is lower than the T_c, the THz emission signal from Ni/$Ni_{70}Cu_{30}$ decreases with the decreasing temperature. Even after inserting a 5-nm-thick Cu layer into the Ni/$Ni_{70}Cu_{30}$ structure, the THz radiation signal remains temperature sensitive, as shown in Figs. 5(c) and 5(d). When the temperature exceeds the Curie temperature, the $Ni_{70}Cu_{30}$ is in the paramagnetic phase. In this case, laser-induced spin currents are generated only in the FM layer, then injected into the $Ni_{70}Cu_{30}$ film and transformed into charge current via ISHE, generating the THz wave. However, as the temperature decreases below T_c, the $Ni_{70}Cu_{30}$ film transitions to the ferromagnetic phase. At this point, the $Ni_{70}Cu_{30}$ layer will also generate spin current and inject it into the FM layer.

If the SHA of the FM layer is as large as that of Ni, the spin current will be converted to charge current via ISHE or anomalous Hall effect (AHE), resulting in THz emission that is the reverse of the previous one. As a result, the overall THz emission signal is weakened. And the increased magnetization of NiCu below T_c is the main reason for the decrease of THz signal. On the other hand, if the SHA of the FM layer is small, such as in CoFeB, the spin current injected into the FM layer from NiCu will not or only rarely be converted into charge current. Thus, it has little effect on the THz signal. In other words, a modest SHA in the FM layer makes TES experiments less disruptive. Therefore, it may be more convenient to use the TES measurement than the FMR measurement to study the ISHE in FM metal.

IV. CONCLUSION

In conclusion, we have systematically studied the THz emission from the 3*d* transition metal in the CoFeB/NiCu heterostructure. At room temperature, the THz wave shows similar features of a spintronic THz emitter and the intensity of the THz emission in the CoFeB/$Ni_{70}Cu_{30}$ heterostructure is up to a half of that of CoFeB/Pt bilayer. We have demonstrated the THz emission is emitted from the spin-to-charge conversion via inverse spin Hall effect. The temperature dependence of THz emission has also been investigated, and the experimental results show that THz emission is not affected by the phase transition of NiCu in the CoFeB/$Ni_{70}Cu_{30}$ structure. This is owing to the small SHA of the CoFeB layer. Our results show that light metal alloys of 3*d* transition elements with large spin Hall angles have the potential to be spintronic THz emitters in both their paramagnetic and ferromagnetic phases, and that THz emission spectroscopy is an effective technique for studying ISHE or AHE in ferromagnets.

ACKNOWLEDGMENTS

This work was supported by the National Natural Science Foundation of China (Grant No. 51627901), National Key R&D Program of China (2020YFA0710100), National Natural Science Foundation of China (Grant No. 12004366), the Anhui Initiative in Quantum Information Technologies (AHY100000), and Key Research and Development Program of Anhui Province (Grant No. 202104A05020012).

[1] B. Ferguson and X.-C. Zhang, Nat. Mater. **1**, 26 (2002).
[2] M. Tonouchi, Nat. Photonics **1**, 97 (2007).
[3] L. Ho, M. Pepper, and P. Taday, Nat. Photonics **2**, 541 (2008).
[4] P. U. Jepsen, D. G. Cooke, and M. Koch, Laser Photonics Rev. **5**, 124 (2011).
[5] S. Koenig, D. Lopez-Diaz, J. Antes, F. Boes, R. Henneberger, A. Leuther, A. Tessmann, R. Schmogrow, D. Hillerkuss, R. Palmer, T. Zwick, C. Koos, W. Freude, O. Ambacher, J. Leuthold, and I. Kallfass, Nat. Photonics **7**, 977 (2013).
[6] G. Mourou, C. V. Stancampiano, A. Antonetti, and A. Orszag, Appl. Phys. Lett. **39**, 295 (1981).
[7] D. H. Auston, K. P. Cheung, and P. R. Smith, Appl. Phys. Lett. **45**, 284 (1984).
[8] Y. C. Shen, P. C. Upadhya, E. H. Linfield, H. E. Beere, and A. G. Davies, Appl. Phys. Lett. **83**, 3117 (2003).
[9] C. W. Berry, N. Wang, M. R. Hashemi, M. Unlu, and M. Jarrahi, Nat. Commun. **4**, 1622 (2013).
[10] B. B. Hu, X. C. Zhang, D. H. Auston, and P. R. Smith, Appl. Phys. Lett. **56**, 506 (1990).
[11] Q. Wu and X. C. Zhang, Appl. Phys. Lett. **67**, 3523 (1995).
[12] X. Mu, I. B. Zotova, and Y. J. Ding, IEEE J. Sel. Top. Quant. **14**, 315 (2008).
[13] J. Dai, X. Xie, and X. C. Zhang, Phys. Rev. Lett. **97**, 103903 (2006).
[14] K.-Y. Kim, J. H. Glownia, A. J. Taylor, and G. Rodriguez, Opt. Express **15**, 4577 (2007).
[15] X. Xie, J. Dai, and X. C. Zhang, Phys. Rev. Lett. **96**, 075005 (2006).
[16] T. Kampfrath, M. Battiato, P. Maldonado, G. Eilers, J. Nötzold, S. Mährlein, V. Zbarsky, F. Freimuth, Y. Mokrousov, S. Blügel, M. Wolf, I. Radu, P. M. Oppeneer, and M. Muenzenberg, Nat. Nanotechnol. **8**, 256 (2013).
[17] T. Seifert, S. Jaiswal, U. Martens, J. Hannegan, L. Braun, P. Maldonado, F. Freimuth, A. Kronenberg, J. Henrizi, I. Radu, E. Beaurepaire, Y. Mokrousov, P. M. Oppeneer, M. Jourdan, G. Jakob, D. Turchinovich, L. M. Hayden, M. Wolf, M. Münzenberg, M. Kläui, and T. Kampfrath, Nat. Photonics **10**, 483 (2016).
[18] Y. Wu, M. Elyasi, X. Qiu, M. Chen, Y. Liu, L. Ke, and H. Yang, Adv. Mater. **29**, 1603031 (2017).
[19] J. Sinova, S. O. Valenzuela, J. Wunderlich, C. H. Back, and T. Jungwirth, Rev. Mod. Phys. **87**, 1213 (2015).
[20] A. Hoffmann, IEEE Trans. Magn. **49**, 5172 (2013).
[21] H. Nakayama, Y. Kanno, H. An, T. Tashiro, S. Haku, A. Nomura, and K. Ando, Phys. Rev. Lett. **117**, 116602 (2016).
[22] M. Isasa, M. C. Martínez-Velarte, E. Villamor, C. Magén, L. Morellón, J. M. De Teresa, M. R. Ibarra, G. Vignale, E. V. Chulkov, E. E. Krasovskii, L. E. Hueso, and F. Casanova, Phys. Rev. B **93**, 014420 (2016).
[23] J. C. Sanchez, L. Vila, G. Desfonds, S. Gambarelli, J. P. Attane, J. M. De Teresa, C. Magen, and A. Fert, Nat. Commun. **4**, 2944 (2013).
[24] R. Schneider, M. Fix, R. Heming, S. Michaelis de Vasconcellos, M. Albrecht, and R. Bratschitsch, ACS Photonics **5**, 3936 (2018).
[25] T. Seifert, S. Jaiswal, M. Sajadi, G. Jakob, S. Winnerl, M. Wolf, M. Kläui, and T. Kampfrath, Appl. Phys. Lett. **110**, 252402 (2017).
[26] L. Cheng, X. Wang, W. Yang, J. Chai, M. Yang, M. Chen, Y. Wu, X. Chen, D. Chi, K. E. J. Goh, J.-X. Zhu, H. Sun, S. Wang, J. C. W. Song, M. Battiato, H. Yang, and E. E. M. Chia, Nat. Phys. **15**, 347 (2019).
[27] E. Vetter, M. Biliroglu, D. Seyitliyev, P. Reddy, R. Kirste, Z. Sitar, R. Collazo, K. Gundogdu, and D. Sun, Appl. Phys. Lett. **117**, 093502 (2020).

[28] X. Wang, L. Cheng, D. Zhu, Y. Wu, M. Chen, Y. Wang, D. Zhao, C. B. Boothroyd, Y. M. Lam, J.-X. Zhu, M. Battiato, J. C. W. Song, H. Yang, and E. E. M. Chia, Adv. Mater. **30**, 1802356 (2018).

[29] H. Zhang, Z. Feng, J. Zhang, H. Bai, H. Yang, J. Cai, W. Zhao, W. Tan, F. Hu, B. Shen, and J. Sun, Phys. Rev. B **102**, 024435 (2020).

[30] M. W. Keller, K. S. Gerace, M. Arora, E. K. Delczeg-Czirjak, J. M. Shaw, and T. J. Silva, Phys. Rev. B **99**, 214411 (2019).

[31] G. Qu, K. Nakamura, and M. Hayashi, Phys. Rev. B **102**, 144440 (2020).

[32] S. Varotto, M. Cosset-Chéneau, C. Grèzes, Y. Fu, P. Warin, A. Brenac, J.-F. Jacquot, S. Gambarelli, C. Rinaldi, V. Baltz, J.-P. Attané, L. Vila, and P. Noël, Phys. Rev. Lett. **125**, 267204 (2020).

[33] X. Tao, Q. Liu, B. Miao, R. Yu, Z. Feng, L. Sun, B. You, J. Du, K. Chen, S. Zhang, L. Zhang, Z. Yuan, D. Wu, and H. Ding, Sci. Adv. **4**, eaat1670 (2018).

[34] S. A. Ahern, M. J. C. Martin, and W. Sucksmith, Proc. R. Soc. A **248**, 145 (1958).

[35] T. S. Seifert, S. Jaiswal, J. Barker, S. T. Weber, I. Razdolski, J. Cramer, O. Gueckstock, S. F. Maehrlein, L. Nadvornik, S. Watanabe, C. Ciccarelli, A. Melnikov, G. Jakob, M. Münzenberg, S. T. B. Goennenwein, G. Woltersdorf, B. Rethfeld, P. W. Brouwer, M. Wolf, M. Kläui, and T. Kampfrath, Nat. Commun. **9**, 2899 (2018).

[36] L. Braun, G. Mussler, A. Hruban, M. Konczykowski, T. Schumann, M. Wolf, M. Münzenberg, L. Perfetti, and T. Kampfrath, Nat. Commun. **7**, 13259 (2016).

[37] J. Yang, S. Jiang, J. Xie, H. Jiang, S. Xu, K. Zhang, Y. Shi, Y. Zhang, Z. Zeng, G. Fang, T. Wang, and F. Su, ACS Nano **15**, 16760 (2021).

[38] See Supplemental Material at http://link.aps.org/supplemental/10.1103/PhysRevB.105.155141 for experimental details, AFM measure, high-resolution HAADF-STEM measure, and magnetic properties of CoFeB/$Ni_{70}Cu_{30}$ structure.

[39] C. Zhou, Y. P. Liu, Z. Wang, S. J. Ma, M. W. Jia, R. Q. Wu, L. Zhou, W. Zhang, M. K. Liu, Y. Z. Wu, and J. Qi, Phys. Rev. Lett. **121**, 086801 (2018).

[40] A. Okada, S. He, B. Gu, S. Kanai, A. Soumyanarayanan, S. T. Lim, M. Tran, M. Mori, S. Maekawa, F. Matsukura, H. Ohno, and C. Panagopoulos, Proc. Natl. Acad. Sci. USA **114**, 3815 (2017).

[41] O. Gladii, L. Frangou, A. Hallal, R. L. Seeger, P. Noël, G. Forestier, S. Auffret, M. Rubio-Roy, P. Warin, L. Vila, S. Wimmer, H. Ebert, S. Gambarelli, M. Chshiev, and V. Baltz, Phys. Rev. B **100**, 174409 (2019).